European Journal of Medicinal Chemistry 200 (2020) 112319

Contents lists available at ScienceDirect

European Journal of Medicinal Chemistry

journal homepage: http://www.elsevier.com/locate/ejmech

Research paper

DDX3X inhibitors, an effective way to overcome HIV-1 resistance targeting host proteins

Annalaura Brai [a, 1], Valentina Riva [b, 1], Francesco Saladini [c], Claudio Zamperini [a], Claudia Immacolata Trivisani [a], Anna Garbelli [b], Carla Pennisi [b], Alessia Giannini [c], Adele Boccuto [c], Francesca Bugli [d, e], Maurizio Martini [f, g], Maurizio Sanguinetti [d, e], Maurizio Zazzi [c], Elena Dreassi [a], Maurizio Botta [a, h, **], Giovanni Maga [b, *]

[a] Dipartimento Biotecnologie, Chimica e Farmacia, Università degli Studi di Siena, Via A. De Gasperi 2, I-53100, Siena, Italy
[b] Istituto di Genetica Molecolare "Luigi Luca Cavalli - Sforza", IGM-CNR, Via Abbiategrasso 207, I-27100, Pavia, Italy
[c] Dipartimento di Biotecnologie Mediche, Università degli Studi di Siena, I-53100, Siena, Italy
[d] Fondazione Policlinico Universitario A. Gemelli IRCCS, Dipartimento di Scienze di Laboratorio e Infettivologiche, I-00168, Roma, Italy
[e] Istituto di Microbiologia, Università Cattolica del SC, L.go F. Vito 1, I-00168, Roma, Italy
[f] Fondazione Policlinico Universitario A. Gemelli IRCCS, Servizio di Istopatologia e Citodiagnosi, Rome, Italy
[g] Istituto di Patologia, Università Cattolica del Sacro Cuore, Rome, Italy
[h] Sbarro Institute for Cancer Research and Molecular Medicine, Center for Biotechnology, College of Science and Technology, Temple University, BioLife Science Building, Suite 333, 1900 N 12th Street, Philadelphia, PA, 19122, USA

ARTICLE INFO

Article history:
Received 29 January 2020
Accepted 6 April 2020
Available online 7 May 2020

Keywords:
DDX3X
Host factors
HIV-1
Antiviral agents
Drug resistance
Coinfections

ABSTRACT

The huge resources that had gone into Human Immunodeficiency virus (HIV) research led to the development of potent antivirals able to suppress viral load in the majority of treated patients, thus dramatically increasing the life expectancy of people living with HIV. However, life-long treatments could result in the emergence of drug-resistant viruses that can progressively reduce the number of therapeutic options, facilitating the progression of the disease. In this scenario, we previously demonstrated that inhibitors of the human DDX3X helicase can represent an innovative approach for the simultaneous treatment of HIV and other viral infections such as Hepatitis c virus (HCV). We reported herein **6b**, a novel DDX3X inhibitor that thanks to its distinct target of action is effective against HIV-1 strains resistant to currently approved drugs. Its improved *in vitro* ADME properties allowed us to perform preliminary *in vivo* studies in mice, which highlighted optimal biocompatibility and an improved bioavailability. These results represent a significant advancement in the development of DDX3X inhibitors as a novel class of broad spectrum and safe anti-HIV-1 drugs.

1. Introduction

The human immunodeficiency virus type 1 (HIV-1) is one of the most devastating viral infections affecting humans and still represents a serious global health issue. Despite antiretroviral therapy (ART) has been introduced in 1996, it has been estimated that 36.7 million persons are living with HIV-1 worldwide, with more than 1 million annual deaths per year [1]. Due to the persistence of latently infected cells and to the high genetic variability, all the efforts to completely eradicate this pathogen or to develop effective prophylactic or therapeutic vaccines have failed so far. Nowadays, thanks to the improved potency of currently available antivirals, HIV-1 replication can be successfully halted in most of treated patients [2]. Unfortunately, ART is life-long and its efficacy can be compromised by the emergence of toxicities, comorbidities and the selection of resistance mutations, which ultimately lead to the progression of the disease [3]. Moreover, immunocompromised patients are susceptible to bacterial, fungal, and viral infections [4,5] complicating their therapeutic regimen with increased pill burden, complex drug interactions and high costs. On these bases,

* Corresponding author. Istituto di Genetica Molecolare "Luigi Luca Cavalli - Sforza", IGM-CNR, Via Abbiategrasso 207, I-27100, Pavia, Italy.
** Corresponding author. Dipartimento Biotecnologie, Chimica e Farmacia, Università degli Studi di Siena, Via A. De Gasperi 2, I-53100, Siena, Italy.
E-mail addresses: botta.maurizio@gmail.com (M. Botta), giovanni.maga@igm.cnr.it (G. Maga).
[1] These authors equally contributed to this work.

https://doi.org/10.1016/j.ejmech.2020.112319

discovery and development of drugs endowed with a new mechanisms of action, non-inferior tolerability, improved pharmacokinetic profile and possibly contributing to reduce the burden of latent cellular reservoir and the chronic immune activation, is of great necessity to improve the quality of existing treatments.

The indirect-acting antiviral agents (IAAs) represent an interesting class of drugs, characterized by a great genetic barrier that make them less susceptible to resistance [6]. In facts viruses exploit the components of the host cells in order to complete their replication, making human cofactors useful targets to develop new antiviral agents [7,8]. The DEAD-box family comprises a large number of human proteins known to be recruited by different viruses [9–11]. In 2004 the ATPase/RNA helicase X-linked DEAD-box polypeptide 3 (DDX3X) has been identified as an indispensable human cofactor for the Rev/CRM1 dependent nuclear export of the unspliced HIV-1 RNAs [12]. Starting from such evidence, in the last ten years we thoroughly analyzed DDX3X structure, identifying ligands able to selectively bind the ATPase or the helicase binding site, increasing their activities and reaching optimal specificity against our target protein. Accordingly, our small molecule DDX3X inhibitors were able to inhibit HIV-1 replication [13–17] (Chart 1). In a previous work we identified compound **EI01D** [15] the first DDX3X inhibitor designed to selectively block the helicase binding pocket by competing with RNA. Through optimization studies we discovered the derivative **16d** [17] (compound **1** of the present paper) that represents the first DDX3X inhibitor with broad spectrum antiviral activity against multiple RNA viruses (Hepatitis C virus, West Nile virus, Dengue virus) including several HIV-1 mutant strains resistant to the current direct acting antivirals (DAAs). According to these features and to the novel mechanism of action, we investigated the biocompatibility and biodistribution (BD) *in vivo* of a selected DDX3X inhibitor.

Since DDX3X is well conserved from yeasts to humans, we performed preliminary *in vivo* studies in rats that share 99% DDX3X sequence identity with humans [18,19]. Despite the promising antiviral activities, as anticipated by our preliminary *in vitro* ADME analysis, the poor aqueous solubility of compound **1** limited its BD in plasma and organs, preventing us from carrying out *in vivo* experiments that require multiple administrations such as sub-chronic toxicity and pharmacodynamics.

In the present study, we designed and synthesized novel derivatives with improved kinetic aqueous solubility with the purpose to ameliorate the BD and the pharmacokinetic (PK) properties of our hit compound.

Due to the unavailability of the DDX3X crystal structure in the active closed conformation, we previously generated a homology model that led us to identify several RNA-competitive inhibitors [16,17,20]. Herein, through our computational model we rationally designed a series of novel derivatives, by inserting polar groups respectively on the side chain at triazole (C4) position or by inserting different hydrogen bond donors on tolyl ring (compounds **15a-e**). The molecules able to retain compound **1** main interactions within the helicase binding site and characterized by increased *in silico* predicted aqueous solubility were then synthesized and validated as inhibitors of the DDX3X helicase activity. 21 novel DDX3X inhibitors were found, and their ADME properties were experimentally confirmed *in vitro*. 11 compounds were then evaluated against HIV-1 infected cells, revealing promising antiviral activities and selectivity indexes (SI). Taking into account ADME parameters, antiviral activity and SI, compound **6b** was selected for further studies. According to its host-protein targeting direct mechanism, the antiviral activity of compound **6b** was confirmed against a panel of HIV-1 resistant strains carrying mutations to currently approved DAAs. Finally, BD, PK and sub-chronic toxicity experiments were performed in mice, revealing optimal tolerability and improved biodistribution.

2. Results and discussion

2.1. Molecular modelling

Twenty-five novel derivatives of compound **1** were rationally designed using the homology model of the closed conformation of DDX3X previously built by us [16]. Compounds were selected on the basis of their docking score and taking into account their predicted absorption, distribution, metabolism, and excretion (ADME) properties calculated with the QikProp software [21]. DDX3X can assume three different conformations, called open, pre-RNA binding and closed conformation [22] and only the closed conformation presents the structural properties competent for the RNA binding. Docking analysis within the RNA binding site was executed using Gold version 5.2. [23], investigating the region with a distance of 10 Å from Arg276. We decided to use a consensus scoring method, with chemscore that has been used as docking fitness function and goldscore as rescore fitness function. For each molecule 100 poses were generated. Visual analysis was performed using Pymol, version 1.8.4.0 [24].

As represented in Fig. 1, the triazole moiety of **15a** forms hydrogen bonds with Arg326, Gly302 and Thr323. The two urea NH-groups form hydrogen bonds with the backbone of Pro274, while the ether-oxygen binds Thr498. The aromatic group is accommodated in a hydrophobic pocket, constituted by Gly473, Val500 and Ala499. Analogously, triazole moiety of **6a** binds the guanidine group of Arg276, while the two urea NH-groups bind the carbonyl group of the backbone of Pro274. The isoquinoline moiety interacts hydrophobically with Gly473, Val500 and Ala499. Compound **6b** takes hydrogen bonds with the backbone of Pro274, while the triazole ring takes contacts with Arg276. As for the previous compound, the isoquinoline moiety is accommodated in a hydrophobic pocket constituted by Gly473, Val500 and Ala499.

Molecular dynamic simulations were executed on the molecules. Amber 16 was used to perform 40 ns of molecular dynamic simulation at the temperature of 300 K. In particular, as showed in Fig. 2, by the root-mean-square deviation (*rmsd)* value (Fig. 2), of **6a, 15a** and **15b**, they are stable in the active site. **6a**, shows rmsd values stabilized around 2.8 Å. The trajectory analysis confirms that the molecule interacts with the side chain of Arg276 and with the backbone of Pro274. During the simulation, the triazole ring takes contact with the backbone of Gly303 while the isoquinoline moiety is accommodated in the hydrophobic region constituted by Gly473, Val500 and Ala499, and the nitrogen atom makes a hydrogen bond with Arg351.

15a is stable in the RNA binding site, despite the increment of rmsd values due to a rotation of phenyl and butyl groups of the molecule in the binding site. **15a** takes contacts with Arg326, Gly302 and Thr323 and other hydrogen bonds are also formed between the urea moiety and the backbone of Pro274 and the side chain of Thr498.

Finally, the trajectory analysis of **6b** shows a compound able to establish long lasting contacts with the amino acids previously described, especially between the urea NH-groups and the backbone of Pro274 and between the isoquinoline group and the side chain of Arg326.

2.2. Chemistry

The general strategy to synthesize the triazole derivatives is shown in Scheme 1. Azide **3** was synthesized from 4-nitroaniline by diazotization reaction. Huisgen 1,3-dipolar cycloaddiction [25,26] with selected terminal alkynes **4a-g** furnished 1, 2, 3-triazoles **5a-g**, subsequent Pd/C mediated hydrogenation led to desired anilines with excellent yields. Finally, target ureas **6a**, **6b**, **7c**, **7g**, **8d**, **9e**, **9f**,

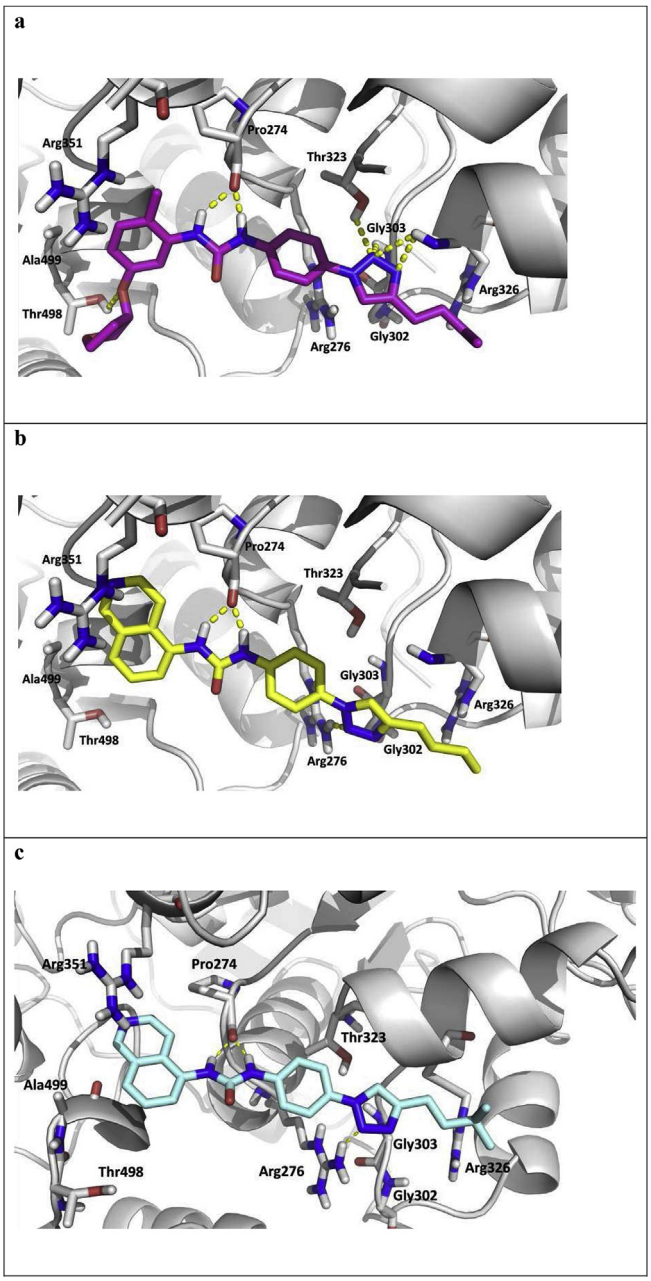

Fig. 1. Binding mode of selected compounds. Molecules were docked in RNA binding site of our in-house built homology model of the closed conformation of DDX3X. (a) In magenta is showed the binding pose of **15a**; (b) in yellow is reported the binding pose of **6a**, (c) in aquamarine is reported the binding pose of **6b**.

10a were produced by treatment with different commercially available isocyanates or with isocyanates synthesized by reacting the opportune aromatic amine with triphosgene with 60–86% yields. Alkyne **4c** was synthesized through Jones oxidation [27] of 4-pentyn-1-ol, **4f** was synthesized by reaction with β-D-ribofuranose 1-acetate 2,3–5 and BF_3 Et_2O as a Lewis acid and **4g** by esterification p-toluensolfonic acid (PTSA) catalysed of **4c**.

As depicted in Scheme 2 aniline **11**, was converted into phenol **12** by Sandmeyer reaction, using the synthetic procedure already reported by Taniguchi et al. [28] and obtaining a comparable yield. Subsequent Mitsunobu reaction with 3-hydroxytetrahydrofuran, or alkylation with cyclopentyl chloride, or phosphorylation in presence of diethylchlorophosphate, o methoxymethylchloride (MOM-Cl) or with β-D-ribofuranose 1-acetate 2,3–5 tribenzoate provided ethers **13a-e** that were reduced and converted into desired ureas **15a-e** as described above. Acidic deprotection of ether **15e** provided phenol **15f**.

With the aim of increasing aqueous solubility several polar groups were introduced on the butyl sidechain, such as amino groups, alcohols, ethers and esters. The synthesis of the series bearing an amino moiety in the aliphatic side chain was performed as depicted in Scheme 3. Alcohols **5h-l** were synthesized by click reaction, activated by tosylation (**16a-c**), and converted into desired amines by nucleophilic displacement. Subsequent reduction Pd catalysed and reaction with the opportune isocyanates provide ureas **20a-c**, **21c** and **22c**. Alcohols intermediates **5h-l** were converted into ureas **23a** and **23b** and subsequently into derivatives **25-27** through Steglich esterification. In order to check the importance of a phosphate in the sidechain, alcohol **23a** was phosphorylated with diethyl chlorophosphate and titanium (IV) isopropoxyde (TTIP) as a Lewis acid (**24a**).

2.3. Biological evaluation

Compounds were tested for their ability to inhibit the helicase activity of DDX3X. Data are presented as half-maximal inhibitory concentration (IC_{50}) and were calculated using a fluorescence resonance energy transfer (FRET)-based assay previously published [17].

As reported in Table 1, the introduction of a planar isoquinolyl ring is well tolerated, being able to hydrophobically interact with Gly473, Val500 and Ala499. Accordingly, compounds **6a** and **6b** reach inhibitory activities of 0.15 and 0.12 μM.

Reverse ester **7g** maintains a good inhibitory activity of 2.02 μM, in contrast its corresponding carboxylic acid **7c** precipitated during the assays.

Ether derivatives **8d** and **9e** retain satisfactory activities of 1.51 and 1.00 μM, in contrast the introduction of ribose in the sidechain abolishes the activity (compound **9f**), probably due to the spatial constrains of the pocket as highlighted in our docking experiment.

In addition, we checked the effect of hydrogen bond acceptor on tolyl ring. Even if the carbonyl group of **10a** establishes an additional interaction with the backbone of Gly473, **10a** presents a small reduction of the activity, probably due to the pocket constrains. Best results were obtained with tetrahydrofuran derivative **15a** that reaches an IC_{50} of 0.10 μM. As already discussed in molecular modelling section, **15a** confirms all the key interactions already seen for compound **1**, in addition the ether-oxygen establishes a hydrogen bond with Thr498. Cyclopentyl derivative **15b**, phosphoric ester **15c** and para methoxymethyl-hydroxy derivative **15e** show high inhibitory activities of 0.14, 0.94 and 0.82 μM. All compounds form the key interactions with Gly302, Arg326 and Thr323, in addition the phenyl ring of **15c** establishes a cation-π interaction with Arg351, while the ether-oxygen of **15e** forms a hydrogen bond with Thr498. Phenol **15f** maintains good inhibitory activity of 0.49 μM, in contrast the introduction of ribose is detrimental for the activity, probably due to the high steric hindrance (compound **15d**).

Alkyl chain at triazole (C4) position was explored by introducing amines. Three different morpholine derivatives were synthesized, increasing the chain length from one to three methylenes (derivatives **20a-c**), in addition we replaced morpholine with methylpiperazine **21c** and N,N-dimethylamine **22c**. As reported in Table 1, the inhibitory activities are directly proportional to the length of the methylene spacer and dimethylamino group is preferred respect to the more hindered morpholino or methylpiperazino moiety. These data confirm our previous published results, which highlighted that linear and long sidechains are preferred with respect to bulky and hindered groups [17,20].

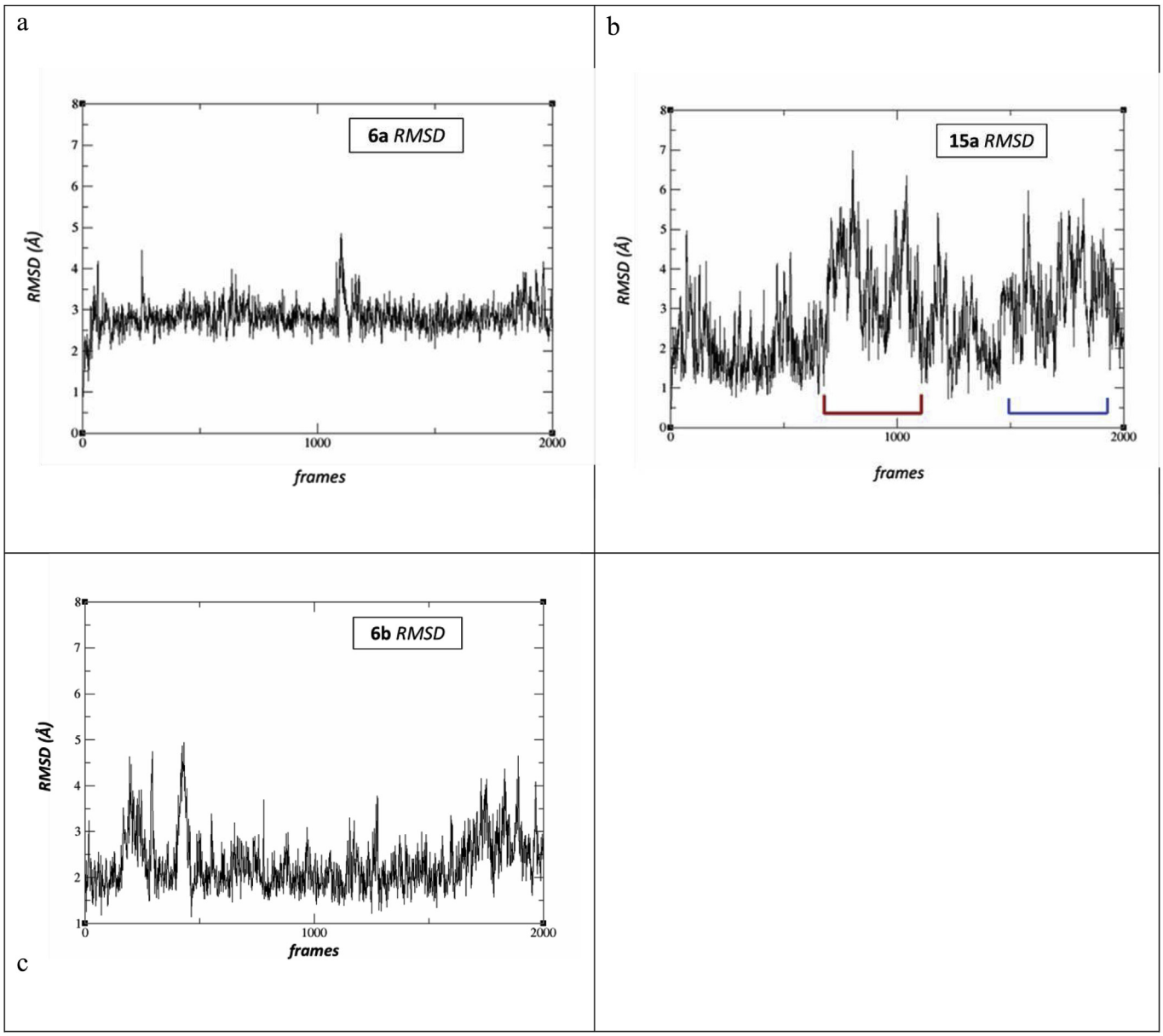

Fig. 2. (a) Plot of the rmsd for **6a**. The plot shows an increasing value for the rmsd, which is stabilized around 2.8 Å. (b) Plot of the rmsd for **15a**. In a first stage, the rmsd oscillates around 2 Å, then, in the red portion, it increases its value. This variation is only caused by the rotation of the phenyl moiety of **15a** and not by the shift of the whole molecule into the binding site. Concerning the blue region, the increase in the rmsd value is due to the movement of the butyl terminal of **15a** into the solvent. (c) Plot of the rmsd for **6b**. Also in this case, the rmsd variation in the first part of the production is due to the rotation of the isopentyl moiety of **6b**, then it stably interacts with the amino acids that constitute the binding site. This behaviour is related to the rmsd value that oscillates around 2 Å during the rest of the simulation.

Accordingly, alcohols **23a** and **23b** are moderately active, probably due to their lower occupancy within the pocket, and maintain the interactions with Gly302 and Pro274. Phosphate ester **24** retains a good inhibitory value, confirming that polar atoms are well tolerated in presence of linear and flexible substituents. In particular, the phosphate ester of **24** establishes a hydrogen bond with Arg276, and the phenyl ring makes a cation-π interaction with Arg480. Among derivatives characterized by the introduction of polar groups on the triazole sidechain the best results were obtained with ester derivatives **25** and **27**, which make an additional hydrogen bond between the carbonyl ester and Arg276. In fact, **25** has an activity of 1.29 μM, and the corresponding trifluoromethyl derivative **26** shows an IC_{50} of 0.40 μM. Ester **27**, due to the presence of the bulkier cinnamic acid moiety, is less active with an IC_{50} of 5.09 μM, that confirmed again our previous findings.

The 9 compounds endowed with the most promising DDX3X inhibitory activities, alcohol **23b** with inhibitory activity below average and compound **15d** completely inactive against DDX3X, were then evaluated through the BiCycle assay as previously described [29]. Briefly, human T cell lymphoma derived clone H9 was infected with HIV-1 wild type NL4-3 strain in presence of serial dilution of compounds. After 72 h, supernatants from each well were used to infect the TZM-bl cell line, which allows the quantitative analysis of HIV infection by measuring the expression of the luciferase gene integrated in the genome of the cells under the control of HIV-1 LTR promoter. Recently, Van Voss et al. [30] reported that the small molecule RK-33 caused lower oxygen consumption rates and decreased intracellular ATP concentrations.

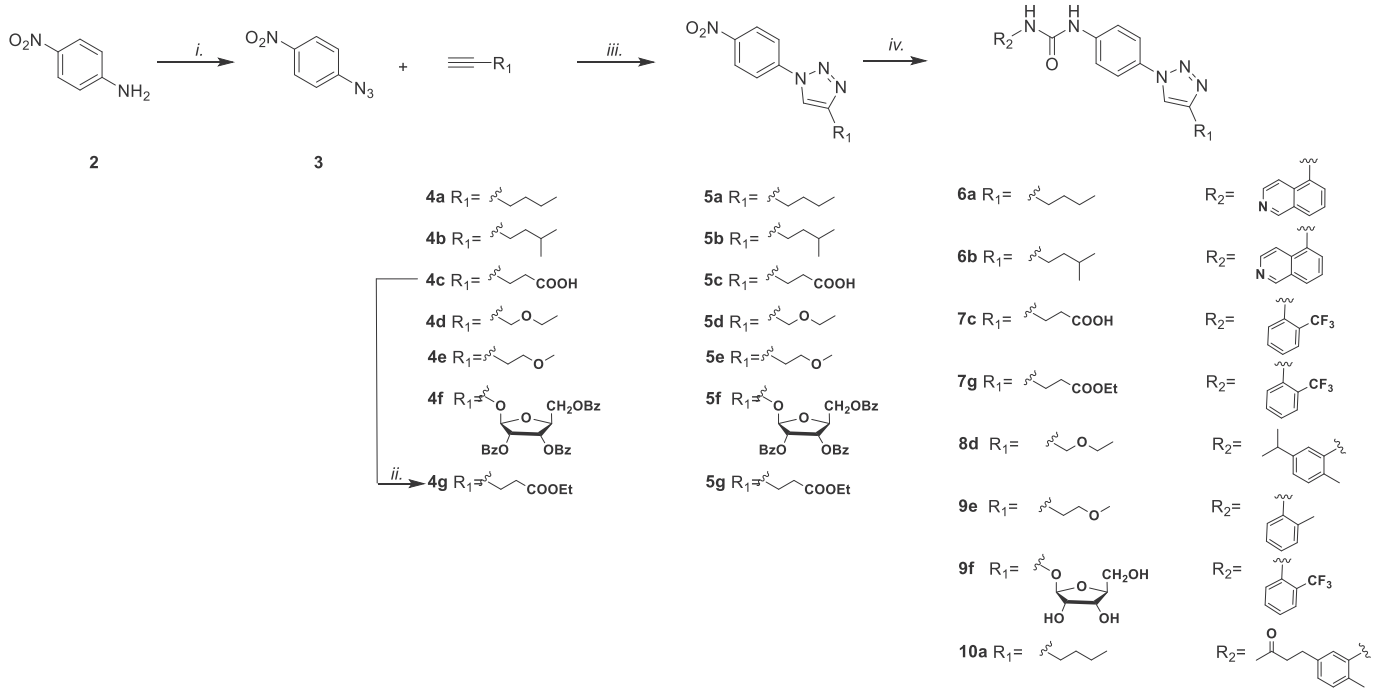

Scheme 1. Synthesis of ureas **6a-10a** modified on triazole sidechain[a]
[a]**Reagents and conditions:** *i.* a) tert-butyl nitrite (*t*-BuONO), CH_3CN, 20 min. 0 °C; b) Trimethylsilyl azide ($TMSN_3$), CH_3CN, 2 h, room temperature (r.t.) (99%); *ii.* PTSA, DCM/EtOH (4:1), 36 h, reflux (80%); *iii.* Alkyne **4a-g**, $CuSO_4 \cdot 5H_2O$, sodium ascorbate, H_2O *t*-BuOH (1:1), MW 120 °C, 300 W, 10 min (70–86%); *iv.* a) H_2, Pd/C, MeOH, 1 h (80–99%), b) opportune isocyanate, CH_2Cl_2, 12 h, r.t. (60–86%).

Taking into account this potential biological effect, we calculated half maximal cytotoxic concentrations (CC_{50}) of our compounds using CellTiter-Glo 2.0 assay (Promega), which evaluates the cell viability by measuring cellular ATP as a marker of the cellular metabolic activity. According to the reported mechanism of toxicity, the CC_{50} of compound **1**, that was previously tested by MTT assay in different cell lines was equal to 90 μM.

As reported in Table 2 compounds **6a** and **6b** and **15b** are characterized by the best antiviral activities, and good selectivity indexes, respectively 36, 41 and 200. Noteworthy, compound **15b** shows an IC_{50} of 0.2 μM, 5-times higher than hit compound **1** already published. Compound **8d** retains appreciable activity and low cytotoxicity, in contrast **15a** and **15c** were found toxic at the concentration of 16 μM. Compound **15d**, which was inserted in the antiviral panel as a negative control, was found inactive at the maximum concentration tested (50 μM). Analogously **23**, probably due to its low inhibiting concentration, does not show any significant activity up to 50 μM. **24** and **26** were surprisingly found inactive, further ADME analysis (see ADME paragraph) demonstrated their high susceptibility to hydrolysis.

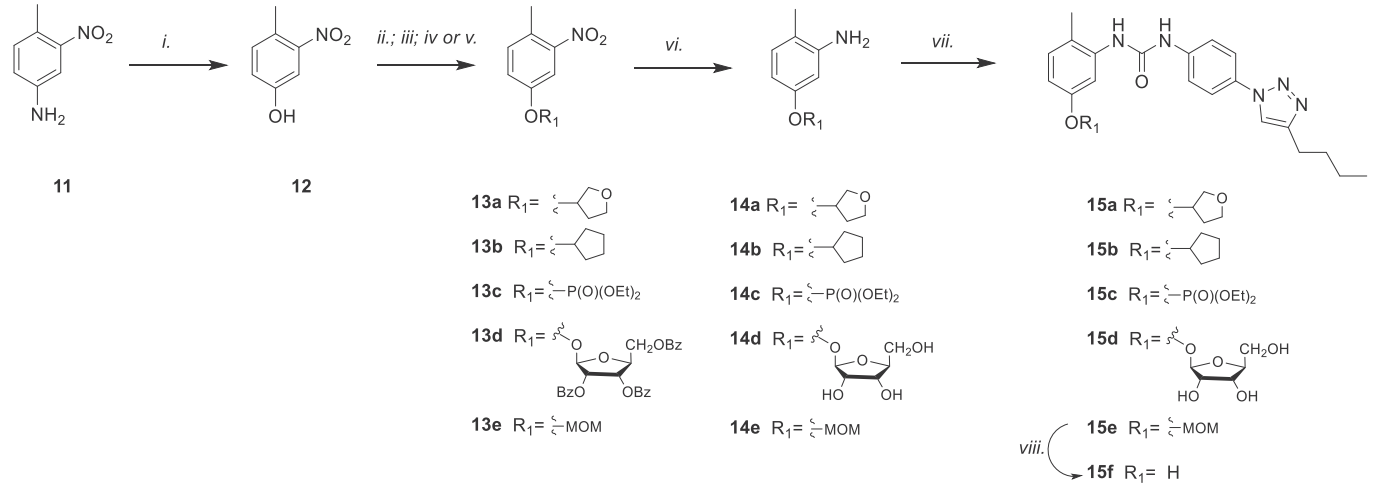

Scheme 2. Synthesis of O-alkylated ureas modified on tolyl ring **15a-e**[aa]Reagents and conditions: *i.* (a) H_2SO_4-H_2O (3:1), 100 °C, 30 min; (b)$NaNO_2$(aq) 0 °C to rt c) 150 °C, 2 h (70%); *ii.* (for **13a**) PPh_3, Diisopropyl azodicarboxylate (DIAD), 3-hydroxytetrahydrofuran, THF, r.t. 9 h (84%); *iii.* (for **13c**) titanium (IV) isopropoxyde (TTIP); diethyl chlorophosphate, TEA, DCM, O/N. r.t.(67%); *iv.* (for **13d**) (a) β-D-ribofuranose 1-acetate 2,3–5 tribenzoate, BF_3 Et_2O 0 °C, CH_2Cl_2,15 min; (b) K_2CO_3 15 min (62%); *v.* (for **13b** and **13e**) (a) NaH, DMF 0 °C to rt (b) cyclopentyl chloride or MOM-Cl, tetrabutylammonium iodide (TBAI), DMF, r.t., 1 h (70–99%); *vi.* H_2, Pd/C, MeOH, r.t., 1 h (99%); *vii.* opportune isocyanate, CH_2Cl_2, 12 h, r.t. (69–79%) *viii.* HCl (3N), MeOH, r.t. 12 h (92%).

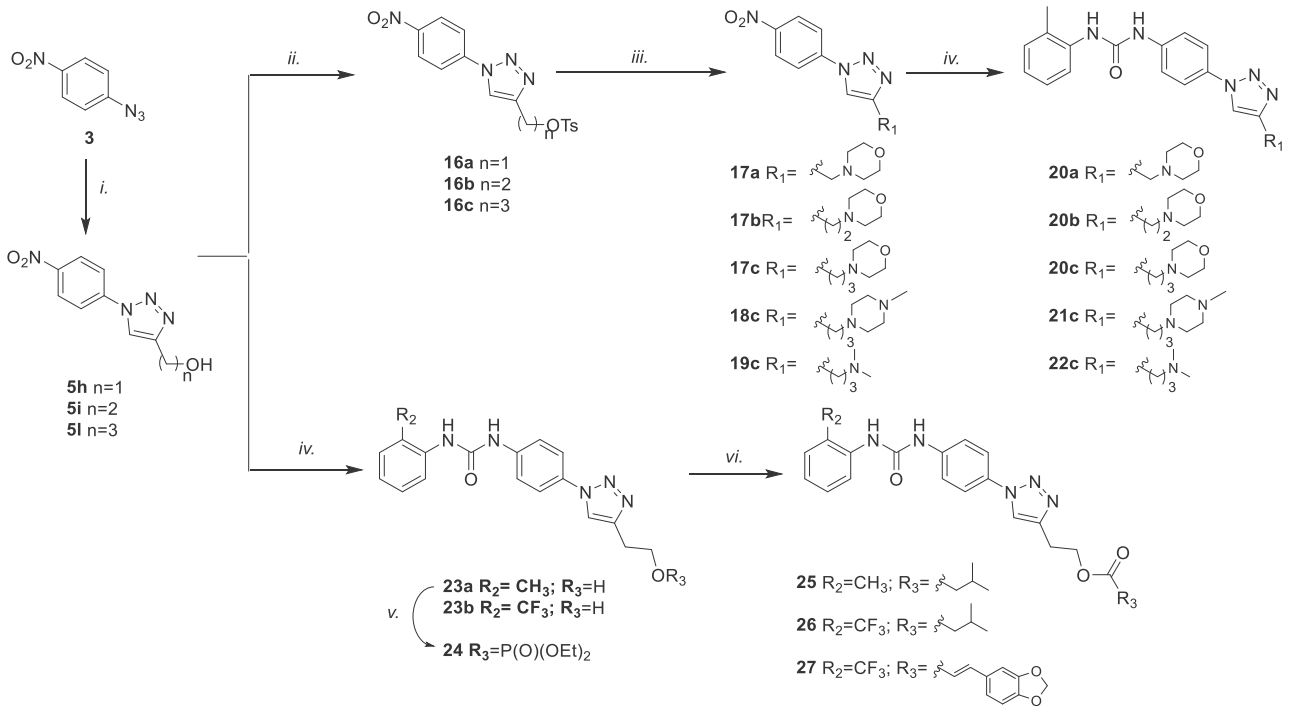

Scheme 3. Synthesis of ureas modified on triazole sidechain[a]
[a]**Reagents and conditions:** *i.* alkyne, $CuSO_4 \cdot 5H_2O$, sodium ascorbate, H_2O tBuOH (1:1), MW 300 W, 10 min, 120 °C (84–90%); *ii.* KOH, TsCl, THF (dry) 24 h, r.t. (72–83%); *iii.* opportune amine, DCM, 9 h, 80 °C (69–95%); *iv* (a) H_2, Pd/C, MeOH, 1 h (99%), (b) opportune isocyanate DCM, 5 h r.t. (67–75%); *v.* TTIP; diethyl chlorophosphate, TEA, DCM o.n. r.t, (75%)*vi.*opportune acid, DCC, DMAP, DCM, DMF 9 h, r.t. (68–74%).

2.4. Activity on HIV-1 resistant strains

Taking into account the low aqueous solubility of **15b** (for details see ADME section), lower than hit compound **1** and outside the recommended range reported for a drug candidate [31], we decided to perform subsequent studies on compound **6b**. Its antiviral activity was evaluated against a panel of HIV-1 strains carrying mutations that confer resistance to the major classes of currently approved antivirals such as protease inhibitors (PIs), nucleos(t)ide reverse transcriptase inhibitors (NRTIs), non-nucleoside reverse transcriptase inhibitors (NNRTIs), integrase inhibitors (INIs) (Table 3). As expected, IC_{50} values are comprised between 1.5 and 2.3 μM, resulting in fold change values ranging from 0.7 to 1.1, clearly confirming that resistant strains are fully susceptible to DDX3X inhibitor **6b**. Results are in agreement with our previously published results [17] and confirm once more the efficacy of IAAs in overcoming viral resistance.

2.5. In vitro ADME analysis

Selected compounds were profiled *in vitro* for aqueous solubility at pH 7.4, liver microsomal stability and membrane passive permeability.

Kinetic solubility was calculated adding 1 mg of compound into 1 mL of water. After 24 h of stirring at 27 °C, the mixture was filtered and the quantity of solubilized compound determined by LC-MS-MS.

As shown in Table 4, except for ether **15b**, accordingly to our *in silico* prediction all the selected compounds showed improved aqueous solubility respect to the parent compound **1**. In fact, ether **15b**, despite its very promising antiviral activity has an aqueous solubility outside the range recommended for a drug candidate. This drawback, already prevented us to perform the repeated toxicological studies with hit **1**, due to the compound's accumulation and to the problems related to its formulation at higher doses. Since repeated administrations are necessary to perform efficacy tests, **15b** was discarded. Except for esters **7g** and **26**, which had only modest improvement of solubility (respectively 3 and 6-times higher), the other compounds were from 10 (isoquinolyl derivatives **6a** and **6b**) to 100-times (**9e** and **15c**) more soluble than **1**.

We then analyzed passive membrane permeability (AppP) using Parallel Artificial Membrane Permeability Assay (PAMPA). Briefly, compound was dissolved in DMSO, diluted with phosphate buffer and placed into the donor compartment of a multi-well microtitre plate. After 5 h of incubation, the quantity of compound able to diffuse from the donor compartment to an acceptor compartment, passing through a semipermeable artificial membrane, was calculated by LC-MS-MS. As reported in Table 4 compounds are characterized by low but non limiting AppP, esters derivatives **7g** and **26** have values comparable or higher than **1**.

Finally, microsomal metabolic stability tests were performed. Each compound was solubilized in DMSO solution and incubated at 37 °C for 60 min in phosphate buffer in presence of human liver microsomes. The reaction mixtures were then centrifuged, and the parent drug and metabolites were subsequently determined by LC-UV-MS. As reported in Table 4 compounds showed good to excellent metabolic stability, with exception of esters derivatives **7g** and **26** which were respectively converted into the corresponding alcohol and carboxylic acid.

2.6. In vivo BD, PK and toxicity studies

Despite the promising antiviral activity of **6b**, its aqueous solubility outside the recommended range coupled with the previous issues related to hit **1** formulation and accumulation in the organs, **6b** was chosen as preclinical candidate. Its low passive permeability, as reported in ADME section, in absence of any information

Table 1
Anti-enzymatic activity of the compounds against the DDX3X helicase[a].

Cmpd.ID	IC_{50}± SD[b](μM)	Cmpd.ID	IC_{50}± SD[b](μM)
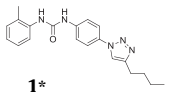 **1***	0.30 ± 0.16	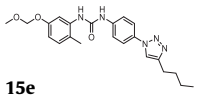 **15e**	0.82 ± 0.12
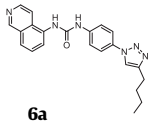 **6a**	0.15 ± 0.09	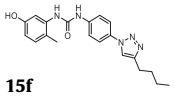 **15f**	0.49 ± 0.10
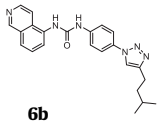 **6b**	0.12 ± 0.10	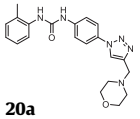 **20a**	na
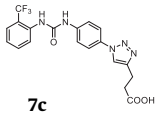 **7c**	nd	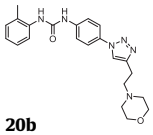 **20b**	59.68 ± 3.0
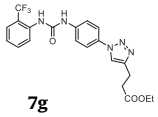 **7g**	2.02 ± 0.7	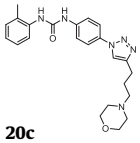 **20c**	53.80 ± 1.1
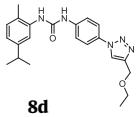 **8d**	1.51 ± 0.8	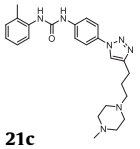 **21c**	40.06 ± 1.7
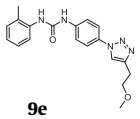 **9e**	1.00 ± 0.5	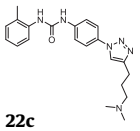 **22c**	2.90 ± 0.2
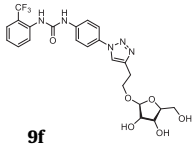 **9f**	na	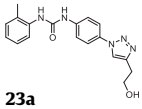 **23a**	13.00 ± 3.1
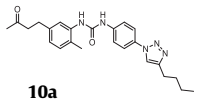 **10a**	2.49 ± 0.7	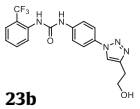 **23b**	11.20 ± 1.2
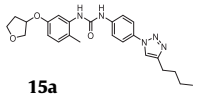 **15a**	0.10 ± 0.07	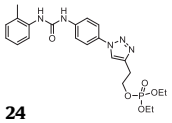 **24**	0.89 ± 0.6
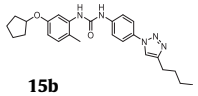 **15b**	0.14 ± 0.05	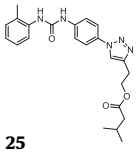 **25**	1.29 ± 2.1
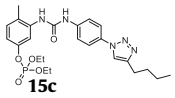 **15c**	0.94 ± 0.12	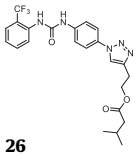 **26**	0.40 ± 0.5

(*continued on next page*)

Table 1 (*continued*)

Cmpd.ID	IC_{50}± SD[b](μM)	Cmpd.ID	IC_{50}± SD[b](μM)
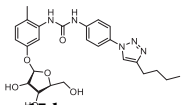 **15d**	na	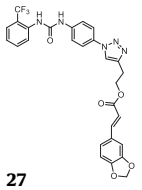 **27**	5.09 ± 0.8

[a] Data represent means values of at least two experiments each performed in duplicate ± S.D.
[b] IC_{50} half maximal inhibitory concentration. na: not active. nd: not determined, compound precipitated from medium.

Table 2
Antiviral activity of selected compounds against HIV-1 infected cells.

Cpd ID[a]	IC_{50}[b] ± SD (μM)	CC_{50}[c] (μM)	SI[d]
1*	1.11 ± 0.5*	90	81
6a	2.2 ± 1.5	80	36
6b	2.1 ± 1.0	86	41
7g	>50	125	–
8d	3.8 ± 1.1	90	24
15a	2.6 ± 1.0	16	6
15b	0.2 ± 0.02	40	200
15c	5.5 ± 1.6	16	2.9
15d	>50	100	–
23b	>50	80	–
24	>50	50	–
26	>50	95	–

[a] Data represent mean ± standard deviation at least two experiments.
[b] IC_{50}: half maximal inhibitory concentration.
[c] CC_{50}: Half maximal cytotoxic concentration.
[d] Selectivity Index (SI): CC_{50} to IC_{50} ratio; *Previously published data.

Table 4
In vitro ADME studies of selected compounds.

Cmpd.ID	AppP[a]	LogS[b]	HLM Stability[c]
1	$2.86 \cdot 10^{-6}$	−7.0	99
6a	$<0.1 \cdot 10^{-6}$	−5.8	95.2
6b	$0.18 \cdot 10^{-6}$	−5.7	89.7
7g	$1.56 \cdot 10^{-6}$	−6.4	16.9
9e	$0.69 \cdot 10^{-6}$	−4.3	94.2
15b	$1.96 \cdot 10^{-6}$	−7.4	92.5
15c	$0.68 \cdot 10^{-6}$	−4.7	85.2
24	$0.72 \cdot 10^{-6}$	−5.4	53.7
26	$4.24 \cdot 10^{-6}$	−6.7	49.3

[a] Apparent permeability reported in $cm \cdot s^{-1}$.
[b] Aqueous solubility expressed as Log of molar concentration.
[c] Human Liver Microsomal Metabolic Stability expressed as percentage of unmodified parent drug.

about its active permeability, led us to investigate its administration using intravenous (i.v.) route. In order to choose the best dose of compound **6b** to be administered, and to identify its concentration in plasma and organs, four groups of 18 Balb/c mice each, were treated with compound **6b**, at the dose of 8 mg/kg, 16 mg/kg or 32 mg/kg and the other received vehicle. Mice were all injected by i.v. administration via tail vein and blood samples were collected at 15 and 30 min and 1, 2, 4, 6, and 24 h. Samples were processed and analyzed by HPLC-MS (For details see methods). The main pharmacokinetic parameters from single-compartment model analysis are summarized in Fig. 3. The half-life elimination and the plasmatic clearance values denoted that **6b** was slowly eliminated after i.v. administration.

Tissues (kidneys, liver, spleen and brain) were collected at 15 and 30 min and 1, 2, 4, 6, and 24 h after i.v. administration of 16 mg/kg and 32 mg/kg of **6b**. Tissue samples were accurately processed and analyzed, results are reported in Fig. 4 (For details see methods). Compound **6b** reached the maximum concentration after 1 h, and was completely eliminated after 24 h. No trace of **6b** was found into the brain, demonstrating its inability to cross blood-brain barrier. As reported by Nolan et al. [32] the spleen may act as a reservoir for HIV thus contributing to the viral persistence. Interestingly, we found important concentrations of **6b** in the spleen, that suggest a potential use of our compound in the reservoir reduction. According to the ADME data, **6b** reached good concentrations, that are in every case major than its IC_{50}. In fact, after 240 min its plasmatic concentration was around 10 μM, 5-times higher than its IC_{50}. After 24 h the plasmatic concentration decreased to 2 μM, suggesting that a daily administration will be necessary in a future efficacy test.

In order to identify potential target organs and toxicities two groups of 10 Balb/c mice each, were treated with **6b** at the highest dose of 32 mg/kg. Mice were all injected by intravenous administration via tail vein, three times a week for three consecutive weeks. Observations were made twice a day for clinical signs of pharmacologic and toxicological effects of the treatment. The body weights of all mice were recorded before the experiment and once every

Table 3
Antiviral activity of compound **6b** against HIV-1 resistant strains.

Virus[a]	Drug class resistance[b]	Resistance mutations	IC_{50} ± SD (μM)[c]	FC[d]
NL4-3	none	none	2.1 ± 0.8	–
11808	PIs	**Major:** V32I, I54V, I84V, L90M **Accessory:** L10F, V11I, K20T, L33F, E35G, A71I, G73S, L89V	2.3 ± 0.1	1.1
7400	NRTIs	M41L, E44D, D67N, T69D, M184V, L210W, T215Y	1.8 ± 0.8	0.8
11847	INIs	G140S, Q148H	1.5 ± 0.1	0.7
12231	NNRTIs	K103N, V179F, Y181C	1.8 ± 0.1	0.8

[a] NIH AIDS Reagent Program catalogue number (www.aidsreagent.org).
[b] PIs: protease inhibitors; NRTIs: nucleos(t)ide reverse transcriptase inhibitors; NNRTIs: non-nucleoside reverse transcriptase inhibitors; INIs: integrase inhibitors.
[c] Antiviral activity calculated with a two round of infection assay.
[d] Fold change values indicate the ratio between IC_{50} values from resistant and wild type strains.

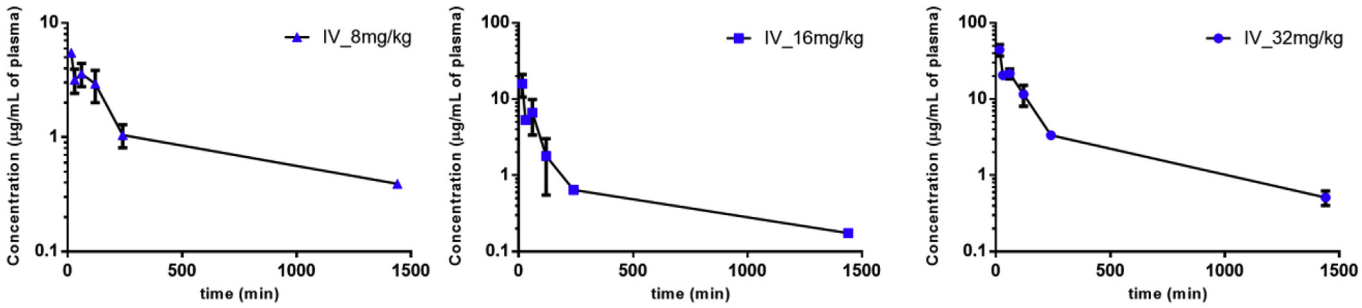

I.V.				
Parameter	Unit	8 mg/kg	16 mg/kg	32 mg/kg
t1/2	min	538.1	465.4	280.9
Cmax	µg/mL	5.5	15.8	44.4
AUC 0-t	µg/mL*min	1536.1	1422.1	5907.2
AUC 0-inf_obs	µg/mL*min	1839.8	1539.3	6114.4
Vz obs	L/kg	3.4	7.0	207.1
Cl obs	mL/min/kg	4.3	8.0	48.0

Fig. 3. Pharmacokinetic analysis. Four groups of 18 Balb/c mice each, were treated with compound **6b**, at the dose of 8 mg/kg, 16 mg/kg or 32 mg/kg. Mice were all injected by intravenous administration via tail vein and blood samples were collected at 15 and 30 min and 1, 2, 4, 6, and 24 h. Samples were processed and analyzed by HPLC-MS.

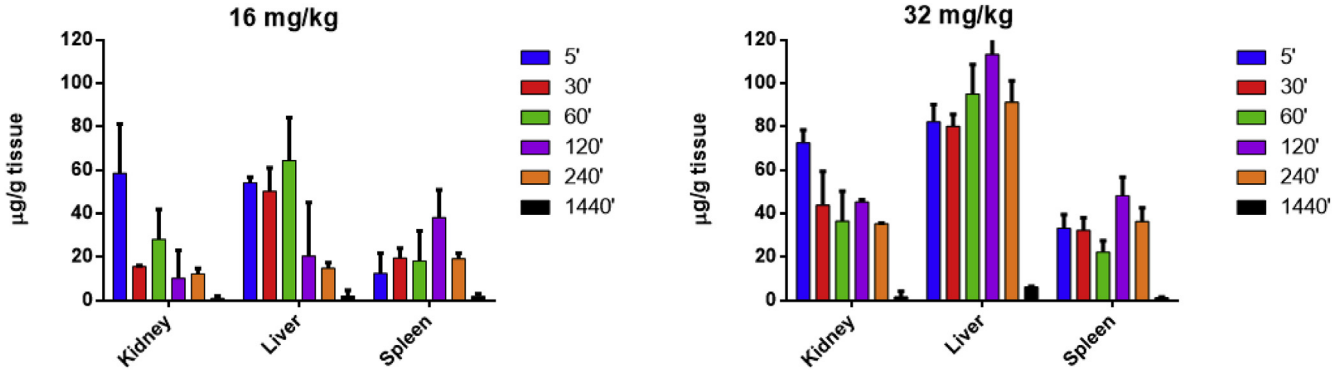

Fig. 4. Biodistribution of 6b in Balb/c mice. Concentration levels of compound in mice tissues at 5, 30, 60, 120, 240 and 1440 min of 6b at the dose of 16 mg/kg, and 32 mg/kg iv.

day after the treatment and showed no significant changes. No animal died before the end point. Two days after the last injections, liver, kidneys and brain were excised from all animals, extensively washed with distilled water and stored at 4 °C in 4% formaldehyde for subsequent analysis. Depth histopathological examination was carried out following necropsy. Organ Samples sections were stained with hematoxylin and eosin (H&E). As highlighted in Fig. 5, no histological alterations were found at the tested dose, demonstrating that **6b** is well tolerated.

3. Conclusions

In the present paper, starting from hit compound **1**, 25 novel potential inhibitors of the helicase activity of the human protein DDX3X were rationally designed using a homology model previously generated by us. The molecules able to retain compound **1** main interactions within the helicase binding site and characterized by increased *in silico* predicted aqueous solubility were then synthesized and validated against DDX3X enzyme. As a result, 21 novel DDX3X inhibitors were found, with inhibitory activities ranging from 0.1 to 60 µM. Eleven compounds were then evaluated against HIV-1 infected cells, by using an *in vitro* phenotypic cell-based assay, revealing activities ranging from the low micromolar to submicromolar range. A preliminary ADME analysis was performed, in order to select the most promising compound for further *in vivo* assays. Compounds metabolically instable or poorly soluble were abandoned. Unfortunately, despite the promising antiviral activity of 0.2 µM, compound **15b** was discarded due to its very low aqueous solubility, which already prevented us to perform subchronic *in vivo* studies. Taking into account ADME parameters, antiviral activity and SI, compound **6b**, 10-times more soluble than hit compound **1,** was selected to perform additional studies. According to its mechanism, directed against a host target, the antiviral activity was retained against a panel of HIV-1 resistant strains carrying resistance mutations in the viral proteins targeted by the currently approved DAAs, with fold changes comprised between 0.8 and 1.1 that demonstrated the full susceptibility to the drug.

Finally PK, BD and subchronic toxicity in mice were carried-out, revealing optimal tolerability and improved biodistribution respect to hit compound **1** previously published [17]. In conclusion, we

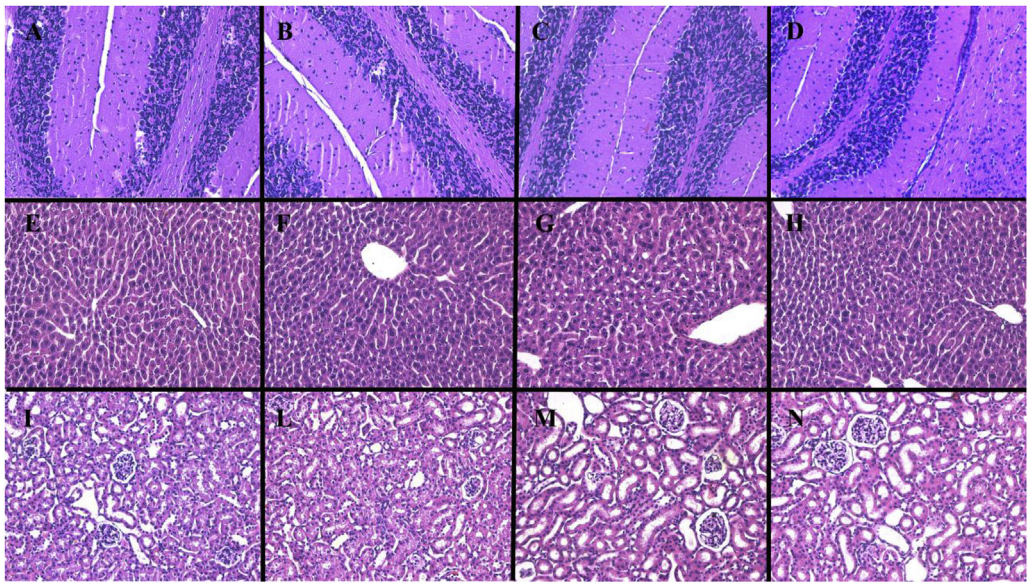

Fig. 5. Representative images of the histological examination of HE-stained sections of Brains (A, B, C, D), A-B: Treated mice, C: Vehicle group, D: Wilde Type group; Liver (E, F, G, H), E-F: Treated mice, G: Vehicle group, H: Wilde Type group; Kidneys (I, L, M, N), I-L: Treated mice, M: Vehicle group, N: Wilde Type group. Treated mice do not exhibit abnormal histopathological changes compared with control groups. The microphotographs were taken using digital camera (Nikon SLR-D3000) at original magnification of 200X.

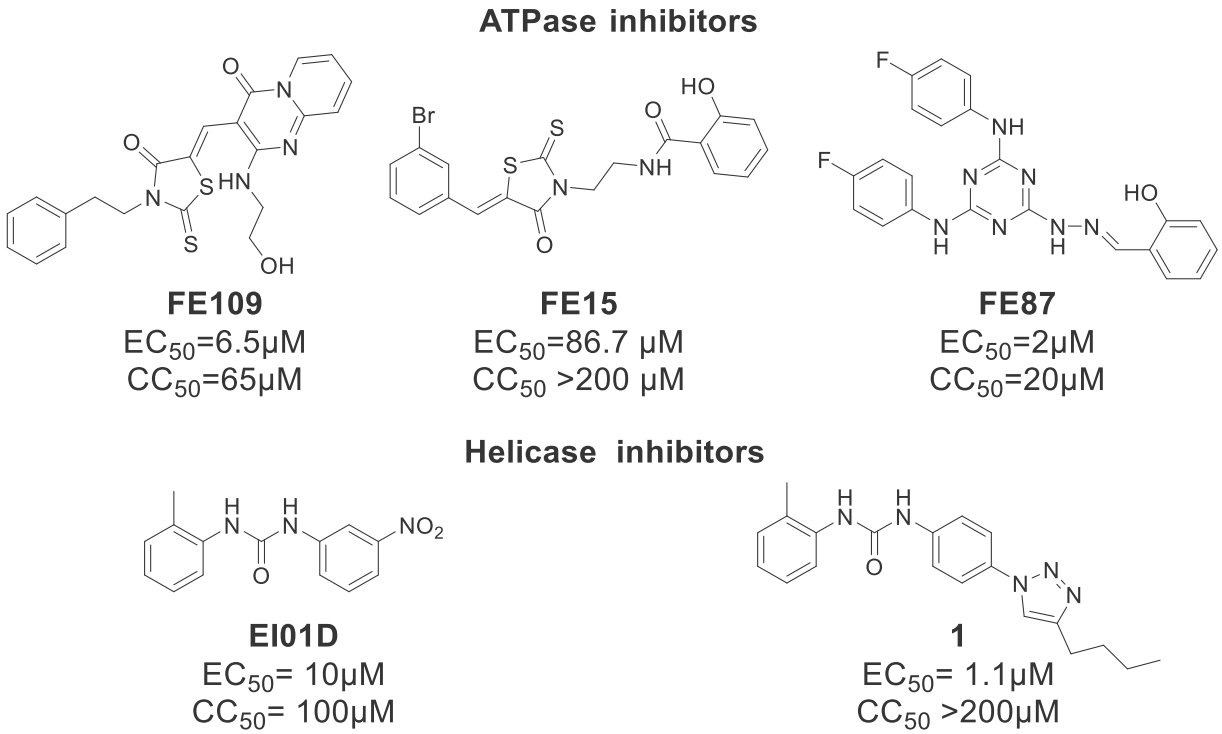

Chart 1. Structures of known DDX3X inhibitors with anti-HIV-1 activity.

report herein a novel promising DDX3X inhibitor, characterized by antiviral activity against HIV-1 wt and resistant strains. *In vivo* results highlighted optimal tolerability and suggest that a daily dose of 32 mg/kg could be used to perform efficacy studies in HIV-1 infected mice, reaching concentrations 4-times higher than IC_{50}. The absence of histological alterations, coupled with the good PK profile and the promising antiviral activity, make **6b** a good candidate for *in vivo* experiments alone or in combination with other drugs with different mechanism of action as a novel strategy to overcome the drug resistance associated with other DAAs. In addition, the high concentration found into the spleen suggested a possible therapeutic use in the reservoirs' treatment. Finally, the SAR reported herein will be taken into account to synthesize novel back-up derivatives with improved ADME properties.

Even if further studies are necessary to prove the efficacy on an animal model of HIV-1 infection, our results pave the way for the

use of host targeting antivirals such as DDX3X inhibitors against viral diseases, in particular in the treatment of resistant strains that are no more susceptible to the DAAs currently available on the market.

Author contributions

MB and GM had the original idea. BA designed, synthesized compounds and wrote the manuscript. VR purified the recombinant DDX3X and performed all the enzymatic assays. FS, AG and AB performed antiviral and cytotoxicity assays. AG and CP helped with protein purification and enzymatic assays. CZ performed ADME assays and pharmacokinetic analysis. CT designed compounds and performed computational analysis. FB, MM and MS performed *in vivo* studies All authors have given approval to the final version of the manuscript.

Notes

This paper is dedicated to the memory of Prof. Maurizio Botta, pioneer in DDX3X research and beloved master.

Declaration of competing interest

The authors declare that they have no known competing financial interests or personal relationships that could have appeared to influence the work reported in this paper.

Acknowledgments

We are grateful to First Health Pharmaceuticals B.V., the exclusive license holder of the DDX3 inhibitors discussed in this paper, for their economic support of MB, MZ, MS, FS and AB. Financial support has been also provided by Tuscany Region Grant FAS Salute 2014 (DD 4042/2014) to MB and MZ. GM and VR were partially supported by the CNR Project "Identification of novel molecules with therapeutic potential against Zika virus and other emerging viruses"

Appendix A. Supplementary data

Supplementary data to this article can be found online at https://doi.org/10.1016/j.ejmech.2020.112319.

Abbreviations

HIV-1	Human Immunodeficiency Virus 1
t-BuONO	tert-Butyl nitrite
$TMeSiN_3$	trimethylsilylazide
IV	Titanium
TTIP	isopropoxide
DCC	N,N′-Dicyclohexylcarbodiimide
DMAP	4-Dimethylaminopyridine
ADME	absorption distribution metabolism and excretion
SAR	structure activity relationships
MOA	mechanism of action
DIAD	Diisopropyl azodicarboxylate
SD	standard deviation
H&E	hematoxylin and eosin
PK	pharmacokinetic
BD	biodistribution
PD	pharmacodynamics
SI	selectivity indexe

References

[1] AIDSinfo | UNAIDS, (n.d.). http://aidsinfo.unaids.org/(accessed September 27, 2018).
[2] F.J. Lee, J. Amin, A. Carr, Efficacy of initial antiretroviral therapy for HIV-1 infection in adults: a systematic review and meta-analysis of 114 studies with up to 144 weeks' follow-up, PloS One 9 (2014), e97482, https://doi.org/10.1371/journal.pone.0097482.
[3] L. Muri, A. Gamell, A.J. Ntamatungiro, T.R. Glass, L.B. Luwanda, M. Battegay, H. Furrer, C. Hatz, M. Tanner, I. Felger, T. Klimkait, E. Letang, G. Isglobal, Development of HIV drug resistance and therapeutic failure in children and adolescents in rural Tanzania: an emerging public health concern, AIDS 31 (2017) 61–70, https://doi.org/10.1097/QAD.0000000000001273.
[4] K. Naidoo, N. Dookie, K. Naidoo, N. Yende-Zuma, B. Chimukangara, A. Bhushan, D. Govender, S. Gengiah, N. Padayatchi, Infection and Drug Resistance Dovepress Recurrent tuberculosis among hIV-coinfected patients: a case series from KwaZulu-natal, Infect. Drug Resist. 11 (2018) 1413–1421, https://doi.org/10.2147/IDR.S150644.
[5] S. Das, J. Opoku, A. Allston, M. Kharfen, Detecting spatial clusters of HIV and hepatitis coinfections, PloS One 13 (2018), e0203674, https://doi.org/10.1371/journal.pone.0203674.
[6] Z. Lou, Y. Sun, Z. Rao, Current progress in antiviral strategies, Trends Pharmacol. Sci. 35 (2014) 86–102, https://doi.org/10.1016/j.tips.2013.11.006.
[7] A. Garbelli, V. Riva, E. Crespan, G. Maga, How to win the HIV-1 drug resistance hurdle race: running faster or jumping higher? Biochem. J. 474 (2017) 1559–1577, https://doi.org/10.1042/BCJ20160772.
[8] C. Tintori, A. Brai, A.L. Fallacara, R. Fazi, S. Schenone, M. Botta, Protein-protein interactions and human cellular cofactors as new targets for HIV therapy, Curr. Opin. Pharmacol. 18 (2014) 1–8, https://doi.org/10.1016/j.coph.2014.06.005.
[9] W.-T. Wang, T.-Y. Tsai, C.-H. Chao, B.-Y. Lai, Y.-H. Wu Lee, Y-box binding protein 1 stabilizes hepatitis C virus NS5A via phosphorylation-mediated interaction with NS5A to regulate viral propagation, J. Virol. 89 (2015) 11584–11602, https://doi.org/10.1128/JVI.01513-15.
[10] M.E. Loureiro, A.L. Zorzetto-Fernandes, S. Radoshitzky, X. Chi, S. Dallari, N. Marooki, P. Lèger, S. Foscaldi, V. Harjono, S. Sharma, B.M. Zid, N. López, J.C. de la Torre, S. Bavari, E. Zúñiga, DDX3 suppresses type I interferons and favors viral replication during Arenavirus infection, PLoS Pathog. 14 (2018), e1007125, https://doi.org/10.1371/journal.ppat.1007125.
[11] V. Meier-Stephenson, T. Mrozowich, M. Pham, T.R. Patel, DEAD-box helicases: the Yin and Yang roles in viral infections, Biotechnol. Genet. Eng. Rev. 34 (2018) 3–32, https://doi.org/10.1080/02648725.2018.1467146.
[12] V.S.R.K. Yedavalli, C. Neuveut, Y.-H. Chi, L. Kleiman, K.-T. Jeang, Requirement of DDX3 DEAD box RNA helicase for HIV-1 Rev-RRE export function, Cell 119 (2004) 381–392, https://doi.org/10.1016/j.cell.2004.09.029.
[13] A. Garbelli, M. Radi, F. Falchi, S. Beermann, S. Zanoli, F. Manetti, U. Dietrich, M. Botta, G. Maga, Targeting the human DEAD-box polypeptide 3 (DDX3) RNA helicase as a novel strategy to inhibit viral replication, Curr. Med. Chem. 18 (2011) 3015–3027. http://www.ncbi.nlm.nih.gov/pubmed/21651478. (Accessed 22 August 2018).
[14] G. Maga, F. Falchi, M. Radi, L. Botta, G. Casaluce, M. Bernardini, H. Irannejad, F. Manetti, A. Garbelli, A. Samuele, S. Zanoli, J.A. Esté, E. Gonzalez, E. Zucca, S. Paolucci, F. Baldanti, J. De Rijck, Z. Debyser, M. Botta, Toward the discovery of novel anti-HIV drugs. Second-generation inhibitors of the cellular ATPase DDX3 with improved anti-HIV activity: synthesis, structure-activity relationship analysis, cytotoxicity studies, and target validation, ChemMedChem 6 (2011) 1371–1389, https://doi.org/10.1002/cmdc.201100166.
[15] M. Radi, F. Falchi, A. Garbelli, A. Samuele, V. Bernardo, S. Paolucci, F. Baldanti, S. Schenone, F. Manetti, G. Maga, M. Botta, Discovery of the first small molecule inhibitor of human DDX3 specifically designed to target the RNA binding site: towards the next generation HIV-1 inhibitors, Bioorg. Med. Chem. Lett 22 (2012) 2094–2098, https://doi.org/10.1016/j.bmcl.2011.12.135.
[16] R. Fazi, C. Tintori, A. Brai, L. Botta, M. Selvaraj, A. Garbelli, G. Maga, M. Botta, Homology model-based virtual screening for the identification of human helicase DDX3 inhibitors, J. Chem. Inf. Model. 55 (2015) 2443–2454, https://doi.org/10.1021/acs.jcim.5b00419.
[17] A. Brai, R. Fazi, C. Tintori, C. Zamperini, F. Bugli, M. Sanguinetti, E. Stigliano, J. Esté, R. Badia, S. Franco, M.A. Martinez, J.P. Martinez, A. Meyerhans, F. Saladini, M. Zazzi, A. Garbelli, G. Maga, M. Botta, Human DDX3 protein is a valuable target to develop broad spectrum antiviral agents, Proc. Natl. Acad. Sci. U.S.A. 113 (2016) 5388–5393, https://doi.org/10.1073/pnas.1522987113.
[18] C.-Y. Chen, C.-H. Chan, C.-M. Chen, Y.-S. Tsai, T.-Y. Tsai, Y.-H.W. Lee, L.-R. You, Targeted inactivation of murine Ddx3x: essential roles of Ddx3x in placentation and embryogenesis, Hum. Mol. Genet. 25 (2016) 2905–2922, https://doi.org/10.1093/hmg/ddw143.
[19] Q. Li, P. Zhang, C. Zhang, Y. Wang, R. Wan, Y. Yang, X. Guo, R. Huo, M. Lin, Z. Zhou, J. Sha, DDX3X regulates cell survival and cell cycle during mouse early embryonic development, J. Biomed. Res. 28 (2014) 282–291, https://doi.org/10.7555/JBR.27.20130047.
[20] A. Brai, F. Martelli, V. Riva, A. Garbelli, R. Fazi, C. Zamperini, A. Pollutri, L. Falsitta, S. Ronzini, L. Maccari, G. Maga, S. Giannecchini, M. Botta, DDX3X helicase inhibitors as a new strategy to fight the West Nile virus infection, J. Med. Chem. 62 (2019) 2333–2347, https://doi.org/10.1021/acs.jmedchem.8b01403.
[21] QikProp, Schrödinger, LLC, New York, NY, (2019)..

[22] P. Schütz, T. Karlberg, S. van den Berg, R. Collins, L. Lehtiö, M. Högbom, L. Holmberg-Schiavone, W. Tempel, H.-W. Park, M. Hammarström, M. Moche, A.-G. Thorsell, H. Schüler, Comparative structural analysis of human DEAD-box RNA helicases, PloS One 5 (2010), https://doi.org/10.1371/journal.pone.0012791 pii: e12791.
[23] M.L. Verdonk, J.C. Cole, M.J. Hartshorn, C.W. Murray, R.D. Taylor, Improved protein-ligand docking using GOLD, Proteins Struct. Funct. Bioinf. 52 (2003) 609–623, https://doi.org/10.1002/prot.10465.
[24] R. Cole, J.C. Nissink, J.W.M. Taylor, Protein-Ligand docking and virtual screening with GOLD, in: Taylor & Francis, Taylor & Francis, Boca Raton, 2005. Virtual Screen. Drug Discov.
[25] R. Huisgen, 1,3-Dipolar cycloadditions, Angew. Chem. 75 (1963) 604–637.
[26] V.V. Rostovtsev, L.G. Green, V.V. Fokin, K.B. Sharpless, A stepwise huisgen cycloaddition process: copper(I)-catalyzed regioselective "ligation" of azides and terminal alkynes, Angew. Chem. Int. Ed. 41 (2002) 2596–2599, https://doi.org/10.1002/1521-3773(20020715)41:14<2596::AID-ANIE2596>3.0.CO;2-4.
[27] K. Bowden, I. Heilbron, E.R.H. Jones, B.C.L. Weedon, Researches on acetylenic compounds. Part I. The preparation of acetylenic ketones by oxidation of acetylenic carbinols and glycols, J. Chem. Soc. (1946) 39–45.
[28] T. Taniguchi, M. Imoto, M. Takeda, T. Nakai, M. Mihara, T. Iwai, T. Ito, T. Mizuno, A. Nomoto, A. Ogawa, Hydrolysis of diazonium salts using a two-phase system (CPME and water), Heteroat. Chem. 26 (2015) 411–416, https://doi.org/10.1002/hc.21275.
[29] F. Saladini, A. Giannini, A. Boccuto, I. Vicenti, M. Zazzi, Agreement between an in-house replication competent and a reference replication defective recombinant virus assay for measuring phenotypic resistance to HIV-1 protease, reverse transcriptase, and integrase inhibitors, J. Clin. Lab. Anal. 32 (2018), e22206, https://doi.org/10.1002/jcla.22206.
[30] M.R. Heerma van Voss, F. Vesuna, G.M. Bol, J. Afzal, S. Tantravedi, Y. Bergman, K. Kammers, M. Lehar, R. Malek, M. Ballew, N. Ter Hoeve, D. Abou, D. Thorek, C. Berlinicke, M. Yazdankhah, D. Sinha, A. Le, R. Abrahams, P.T. Tran, P.J. van Diest, V. Raman, Targeting mitochondrial translation by inhibiting DDX3: a novel radiosensitization strategy for cancer treatment, Oncogene 37 (2018) 63–74, https://doi.org/10.1038/onc.2017.308.
[31] C.A. Lipinski, Drug-like properties and the causes of poor solubility and poor permeability, J. Pharmacol. Toxicol. Methods 44 (2000) 235–249, https://doi.org/10.1016/S1056-8719(00)00107-6.
[32] D.J. Nolan, R. Rose, P.H. Rodriguez, M. Salemi, E.J. Singer, S.L. Lamers, M.S. McGrath, The spleen is an HIV-1 sanctuary during combined antiretroviral therapy, AIDS Res. Hum. Retrovir. 34 (2018) 123–125, https://doi.org/10.1089/AID.2017.0254.